JMEPEG (2021) 30:9029–9037
https://doi.org/10.1007/s11665-021-06128-x

1059-9495/$19.00

Influence of the Evolution of 9CrMoCoB Steel Precipitates on the Microstructure and Mechanical Properties during High-Temperature Aging

Yulin Ma, Chengyang Kuang, Jun Cheng, and Changdi Yang

Submitted: 29 December 2020 / Revised: 8 June 2021 / Accepted: 23 June 2021 / Published online: 3 September 2021

In this study, the short-term aging was carried out to reveal the evolution of precipitates and mechanical properties of heat resistant 9CrMoCoB steel during the early creep, replacing the conventional creeping. The tempered martensite lath structure (TMLS) and precipitates were observed in the as-aged 9CrMoCoB steel. TMLS in the matrix underwent a transition to the polygonal ferrite after aging only for 300 h. In comparison, the mean diameter of the precipitates increased from 183 to 267 nm after aging at 650 °C for 300 h. Also, the mean diameter of the precipitates increased from 183 to 302 nm at 700 °C. The room-temperature and high-temperature strength of 9CrMoCoB steel decreased after high-temperature aging, which may be mainly due to precipitates coarsening. Many $M_{23}C_6$ phases precipitate in the prior austenite grain boundary (PAGB) and lath boundary. After aging 100 h, TMLS transformed into polygonal ferrite, and the size of the precipitate at the subgrain boundary was about 100 nm, while after 300 h of high-temperature aging, large precipitates appear (400 nm) in the matrix. After 200 h of high-temperature aging, the obvious growth of precipitates on the PAGB and lath boundary weakens the pinning effect on the PAGB and martensite lath boundary and accelerates the transformation of microstructure and mechanical properties.

Keywords 9CrMoCoB steel, grain boundary, high-temperature aging, mechanical properties, precipitate

1. Introduction

An ultra-supercritical (USC) unit in a thermal power plant can effectively reduce energy consumption and pollution. Owing to its importance, studies are continuously focused on ultra-supercritical steel materials (Ref 1, 2). During the end of the last century, the European research institute (Ref 3, 4) has developed 9CrMoCoB steel (Ref 5-7) based on P92 steel (Ref 8-10) by increasing the content of B (Ref 11, 12) and introducing Co (Ref 13-15).The main steam pipelines of power plants in the United States target continuous use of 100,000 h by utilizing steam at 100 MPa (Ref 16, 17). After the creep test for 85,000 h, it has been found that 9CrMoCoB steel has good creep resistance, and hence it is considered a key material for thermal power plant unit castings (Ref 3). The key problem of heat resistant steel materials in operation is that the evolution of internal microstructure occurs under high temperature and pressure for a long time, such as coarsening the precipitated phase and the movement of martensite lath boundary (Ref 18-21).

Few studies reported that the Z phase in the 9CrMoCoB matrix appears after aging for 67,857 h, and the formation of the Z phase consumes V, Nb, leading to a decrease in the strengthening of precipitate (Ref 22-24). The 9CrMoCoB steel was subjected to a steam temperature of 650 °C and a steam pressure of 50 to 120 MPa, and their longest service periods were 67,857 h and 82,649 h, respectively. The evolution of the precipitated phases occurred during the service. Laves phase nucleates at the boundary of $M_{23}C_6$ carbide and grows quickly (Ref 25). Some researchers often use static aging instead of creep experiments to investigate the microstructure and mechanical properties of the evolution (Ref 16, 26-30). Zielinski (Ref 31) studied the mechanical properties and microstructure of P92 steel at 600 and 650 °C after 100,000 h. It was found that an increase in the number and size of $M_{23}C_6$ carbides could also assess the microstructure evolution of test steels. This method is considered useful for assessing the performance of boiler material under long-term high-temperature and high-pressure conditions. It has been found that the evolution behavior of carbides in the microstructure during service has become an important factor that affects the mechanical properties (Ref 32, 33). The rapid growth of carbides in the matrix can reduce the content of solid solution elements and decrease the pinning effect of dislocations, which is the main reason for reducing the service life of materials (Ref 34).

9CrMoCoB steel exhibits good creep resistance at 625 °C (Ref 3). However, the evolution in carbide precipitation and mechanical properties of 9CrMoCoB steel during the early creep is rarely reported. In this investigation, the short-term

Yulin Ma, Key Laboratory of Research and Application of Multiple Hard Films, Liaoning Province, School of Mechanical Engineering, Shenyang University, Shenyang 110044, China; and School of Materials Science and Engineering, Northeastern University, Shenyang 110819, China; **Chengyang Kuang** and **Changdi Yang**, Key Laboratory of Research and Application of Multiple Hard Films, Liaoning Province, School of Mechanical Engineering, Shenyang University, Shenyang 110044, China; and **Jun Cheng**, Shaanxi Key Laboratory of Biomedical Metal Materials, Northwest Institute for Nonferrous Metal Research, Xi'an 710016, China. Contact e-mails: mayulin@syu.edu.cn and chengjun_851118@126.com.

static aging experiment instead of the creep experiment was used to examine the carbide precipitation and mechanical properties of 9CrMoCoB steel evolution and the relationship between the impacts, especially on the influence of temperature and holding time on carbide precipitation and performance evolution was examined.

2. Experimental Procedure

2.1 Sample Preparation and Plastic Deformation

The experimental 9CrMoCoB steel was prepared by smelting using a vacuum induction furnace, and the composition was measured by ICP-OES, as shown in Table 1. The steel ingot was forged at 1200-900 °C to obtain a round bar with a diameter of 25 mm and heated at 1100 °C for 2 h followed by air cooling and heating at 730 °C for 2 h and then furnace cooling. After heat treatments, the round bar was aged between 650 and 700 °C. The round bar was aged for 100 to 300 h by subjecting to high temperature continuously, at an interval of every 100 h. The round bar under different temperatures and holding times was processed into tensile specimens for room temperature and high-temperature experiments.

2.2 Characterization of Microstructure

The mixed solution of $FeCl_3$+HCl+alcohol corroded the metallographic samples, and the prior austenite grain size (PAGs) of the test steel was etched by the electrolyte (Ref 16) and was observed using an OLYMPUS DSX-500 optical microscope (OM). Transmission electron microscope (TEM, Tecnai G20) and scanning electron microscope (SEM, Ultra Plus field emission scanning electron microscope) were employed to observe the microstructural morphology (Ref 24). The TEM test samples were prepared by double spray electrolysis, and the electrolyte was an alcoholic solution of $HClO_4$ (8%). In the SEM, electron backscatter diffraction (EBSD) was used to observe the microstructural information (Ref 35). Under different conditions, the precipitated phase was electrolytically extracted in 3.6%$ZnCl_2$ +5%HCl +1%$C_6H_8O_7$ +90.4% CH_3OH solution. The Bettersize 2000 Laser particle size analyzer was used to measure the number and size of the precipitated phase. On the specimens with a diameter of 5 mm and a gage length of 30 mm, room temperature and high temperature (650 °C), tensile tests at a strain rate of 0.8 mm/min were carried out using the SANS universal testing machine (Ref 27).

Table 1 The main chemical elemental content of 9CrMoCoB steel (mass fraction/%)

C	Si	Mn	Cr	Mo	Co	B	Fe
0.13	0.25	0.9	9.5	1.5	1.02	0.009	Bal.

3. Results and Discussion

3.1 Original Microstructure of 9CrMoCoB Steel

A significant amount of fine precipitates can be observed on the martensite matrix. No considerable difference in the size between the precipitates in the grain boundaries and the grain interior can be noted (Fig. 1a). The morphology of the austenite grain boundary (PAGB) after the electrolytic etching+polishing process is shown in Fig. 1(b). Using a metallographic microscope, four nonadjacent points were selected for each sample, and five images were taken at each point, which illustrates that the average PAGs is about 70 μm before aging. Normally, the size of austenite grains after liquid solidification can reach hundreds of microns with irregular shapes. Still, after forging deformation and heat treatment, fine recrystallized austenite grains are formed with uniform size. To facilitate the observation of the growth behavior of the austenite grains during the high-temperature aging process, the experimental steel was forged and deformed. It is shown Fig. 1(b) that the austenite grain size before high-temperature aging is uniform, where the cross-sectional surface is in the direction of deformation.

The TEM image of the original 9CrMoCoB steel demonstrates an obvious TMLS structure (Fig. 2). The precipitates in the lath boundary of the 9CrMoCoB steel after tempering is the $M_{23}C_6$ phase (Ref 36). The precipitate consists $(Cr,Fe)_{23}(C,B)_6$ with a flat shape. In contrast, the small spherical particles near the flake precipitate phase comprise V(C,N), and generally, the precipitate containing small spherical particles is present inside the PAGB. The MX phase (Ref 37, 38) is the high-temperature phase, which is the favorable phase for the material's creep resistance. Many dislocations at the lath boundaries increase the substrate-free energy, providing a diffusion channel and activation energy for the migration of lower single atom and offering a favorable position for the precipitation nucleation. Hence, the precipitation occurs mostly in the lath boundaries. In the high-temperature tempering process, thermal activation transition occurs at the lath boundaries.

3.2 Effect of Aging Condition on the Microstructure

Figure 3 exhibits the EBSD image of 9CrMoCoB steel before and after aging, where the martensitic structure can be observed, along with a large amount of small-angle PAGs before aging. Through comparing the obtained data, it could be seen that there is no significant difference in the number of large-angle as well as small-angle grain boundaries in the samples before and after high-temperature aging. High-angle grain boundaries are generally considered to be PAGB, while small-angle grain boundaries are generally considered to be the substructure within the PAG. Thus the grain size of prior austenite does not change significantly before and after high-temperature aging. The number of small-angle grain boundaries after aging at 650 °C for 300 h is lower than at 700 °C, which might be due to the evolution of the microstructure. This phenomenon is characterized by the evolution of 9CrMoCoB steel in the process of high-temperature aging. Furthermore, some ferrite subgrains could be seen after aging 300 h.

The morphology of the precipitates under different aging conditions is shown in Fig. 4, confirming that the size of the precipitates increases after aging. The precipitate exhibits a similar size after aging at 650 °C for 100 h. The size of the

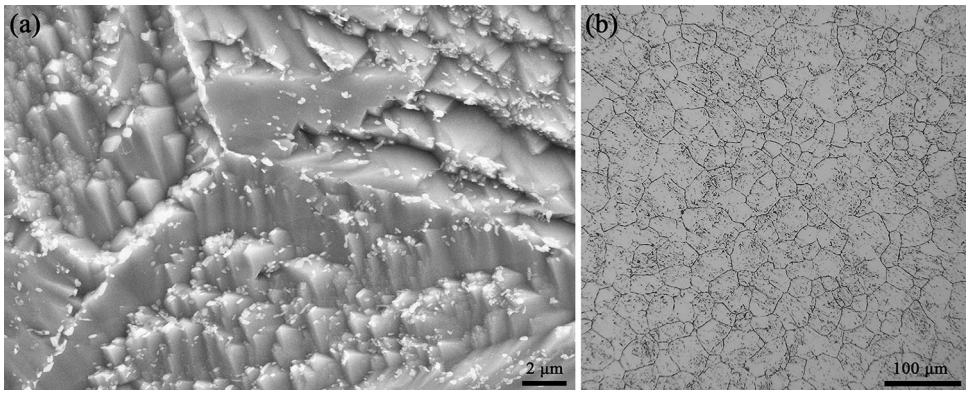

Fig. 1 The morphology of (a) microstructure and (b) PAGB before aging

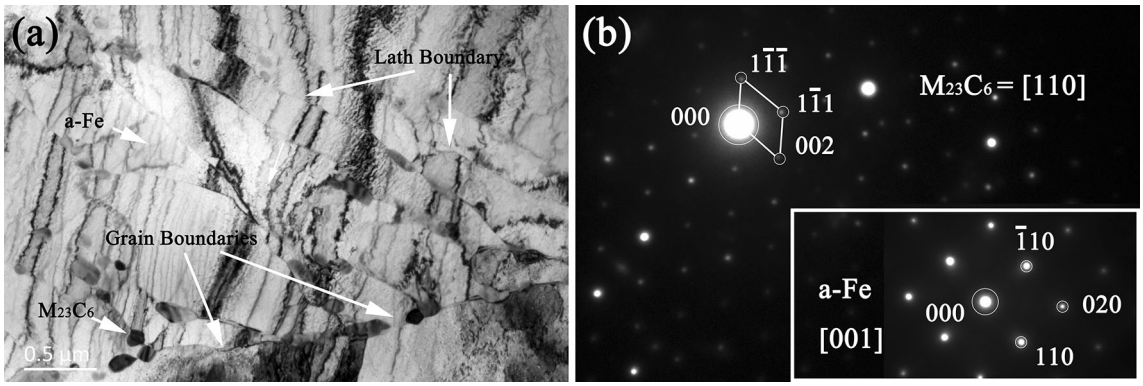

Fig. 2 (a) Bright field micrograph and (b) diffraction pattern of 9CrMoCoB steel before aging

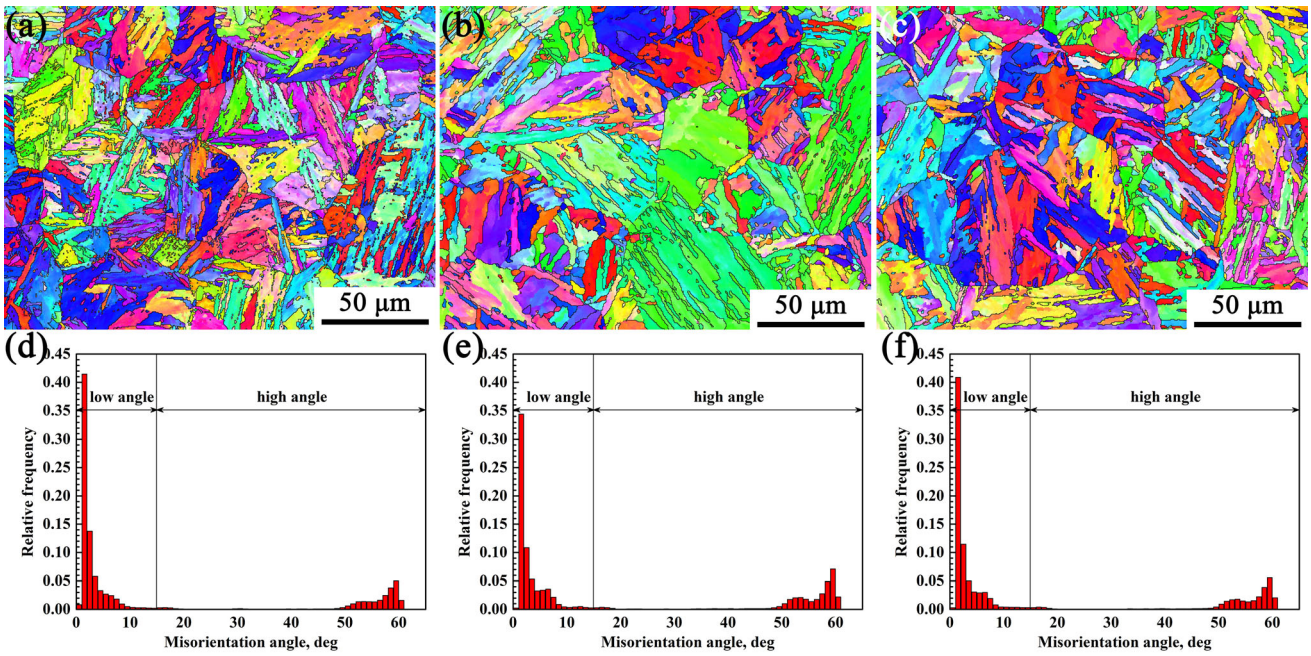

Fig. 3 Orientation map of 9CrMoCoB steel (a) before aging (b) 650 °C after 300 h and (c) 700 °C after 300 h; misorientation angle distribution of 9CrMoCoB steel (d) before aging (e) 650 °C after 300 h and (f) 700 °C after 300 h

precipitate on the PAGB increases with an increase in the aging time. The size of the precipitates is larger at 700 °C than 650 °C. Precipitates with a diameter of ~1 μm could be observed after aging at 700 °C for 300 h (Fig. 4f). The number of precipitates decreased after aging for 300 h, and the precipitate coarsening occurs at high temperatures. These

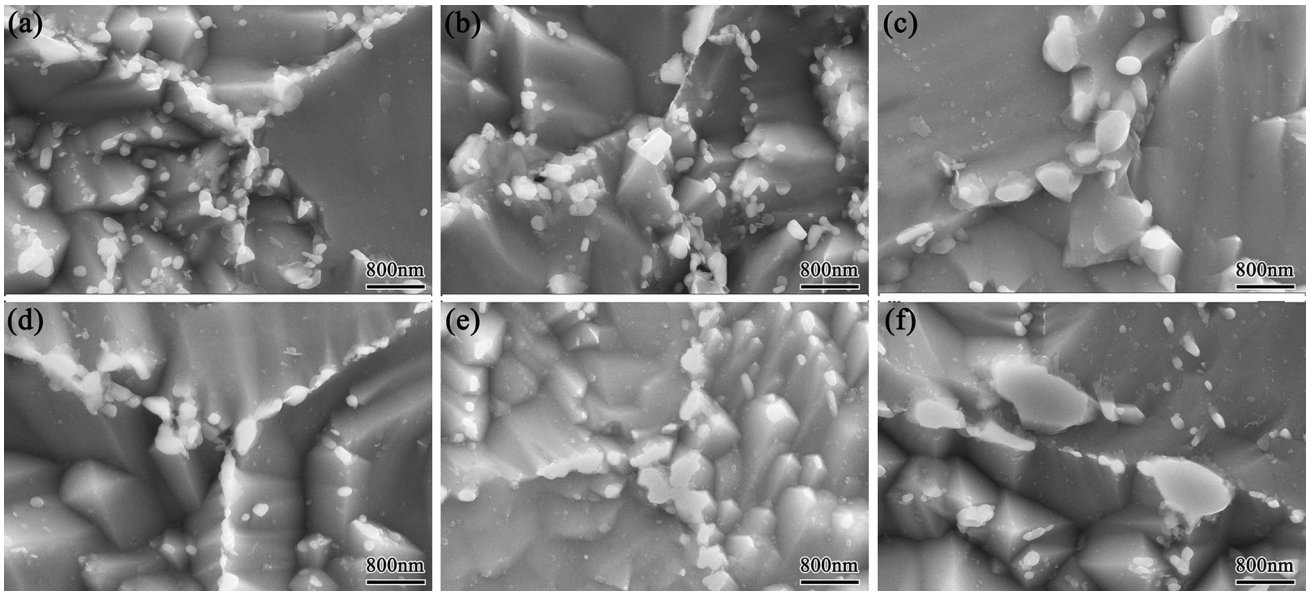

Fig. 4 SEM images of 9CrMoCoB steel after aging (a) 650 °C, 100 h (b) 650 °C, 200 h (c) 650 °C, 300 h (d) 700 °C, 100 h (e) 700 °C, 200 h (f) 700 °C, 300 h

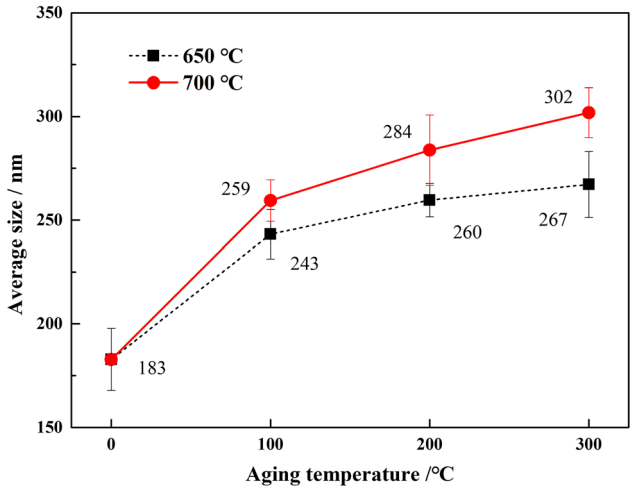

Fig. 5 The size of the precipitation phase of 9CrMoCoB steel under different aging conditions

precipitates dissolve inside the grains and grow rapidly at the grain boundaries, a typical precipitate coarsening phenomenon. The chemical potential gradient controls the transition of alloying elements from a low-concentration solid solution state to a high-concentration precipitate. Under high-temperature aging, alloying elements form precipitates reduce the system's Gibbs free energy. The diffusion of alloying elements in the matrix mainly relies on the PAGB and lath martensite boundaries. The PAGB serves as the surface defects to provide a fast path for diffusion. The PAGB belongs to the high-angle grain boundary, and the martensite lath block substructure has the low-angle grain boundary. The distribution and number of high-angle and low-angle grain boundaries are shown in Fig. 3. The precipitate on PAGB has more elements than the area inside the grain which grows up quickly.

The precipitates were extracted by the electrolysis, and the effect of aging conditions on their size is shown in Fig. 5. With an increase in aging time, the precipitate mean diameter increased from 183 to 267 nm after aging at 650 °C. The precipitate mean diameter increased from 183 to 302 nm at 700 °C, indicating that the aging temperature has an obvious effect on the size of the precipitate. The change in the precipitate size is most significant in the high-temperature aging for the first 100 h, which is due to the large amount of Cr still exists as a solid solution in the matrix after the tempering of the test steel. The precipitate size increases after high-temperature aging for 200 h due to precipitate coarsening. The precipitation temperature of $M_{23}C_6$ in the test steel is slightly higher than 700 °C, one of the main reasons for the more likely precipitate coarsening at 700 °C. As one of the main ways to improve the strength and plasticity of materials, grain refinement mainly depends on the average size of PAGs and lath boundaries (the boundary of the substructure inside the prior austenite grain). The smaller the size of the precipitates, the greater the constraints on the PAGB and lath boundaries. Figure 4 displays the development of the precipitates. Thus, the binding force on the PAGB and lath boundaries weakens, and the growth of the substructure inside the prior austenite grain occurs as the size of the precipitates increases.

The precipitated phase in 9CrMoCoB steel after aging for 300 h is shown in Fig. 6. The SEM-EDS line scan analysis shows that almost all the precipitates are spherical after aging at 650 °C for 300 h (Fig. 6a). The precipitates are mainly Cr-rich carbides (Fig. 6b), and the contents of Cr and Fe are in the transition zone between the carbides and the matrix. This is due to the enrichment of the Cr element near the precipitate but without forming $M_{23}C_6$. The precipitate with a size of about 500 nm is carbide rich with Cr and Mo (Fig. 6c). A large strip with more than 500 nm and a square precipitate of 200 nm appears in the matrix. The line scanning analysis results show that large and square precipitates are carbides and carbonitrides, respectively. This carbonitride is an MX-precipitate rich in V and Nb. After aging for 300 h, the precipitation phenomenon is observed on PAGB, especially at the trigeminal grain boundary,

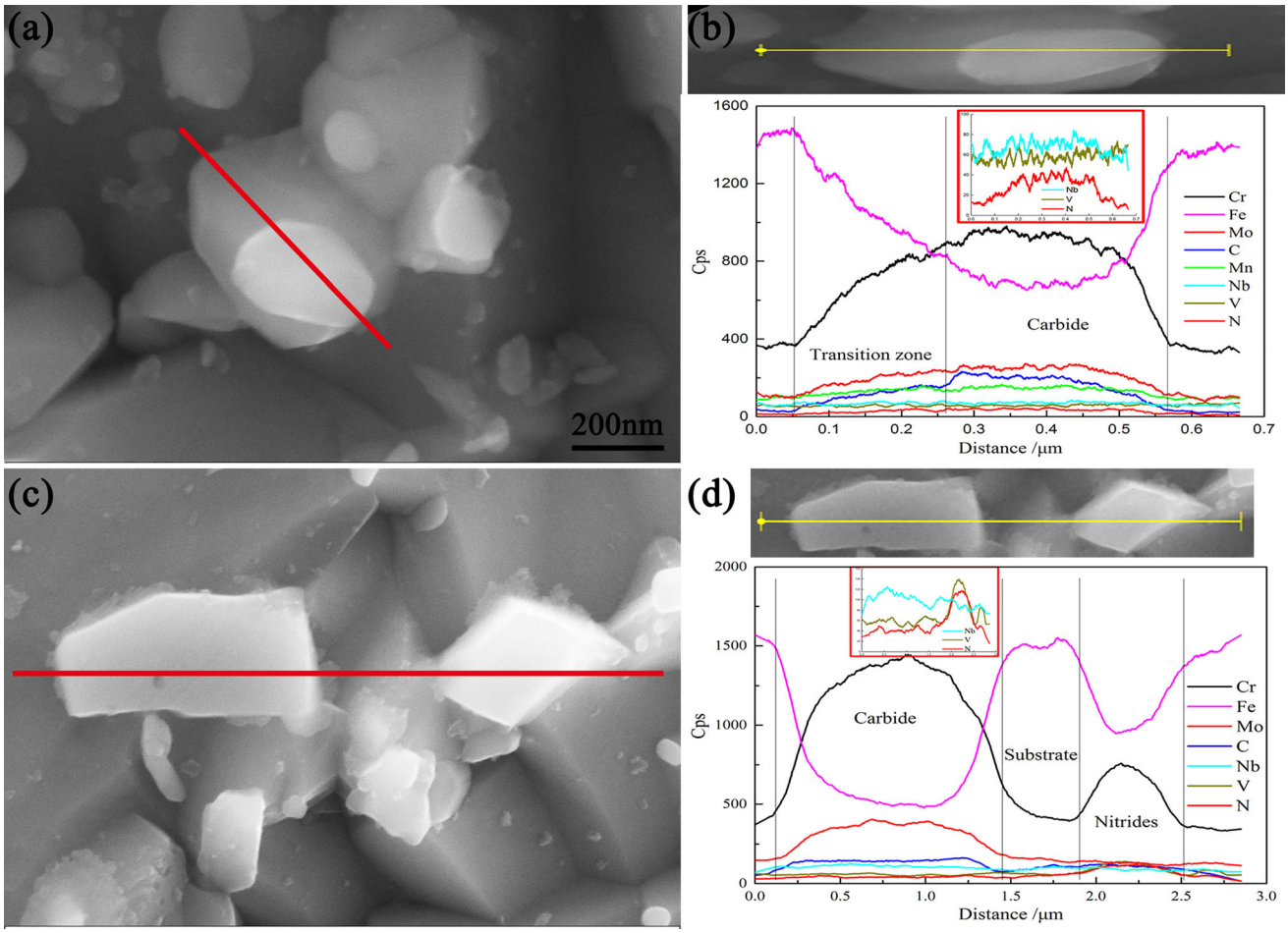

Fig. 6 SEM-EDS line scan analysis of the precipitation phase of 9CrMoCoB steel after aging 300 h (a) 650 °C (b) EDS spectrum (c) 700 °C (d) EDS spectrum

which provides a good precipitation particle for the solid solution element and promotes the precipitate's rapid growth.

The TEM images of the sample after high-temperature aging are shown in Fig. 7. The lath martensite is observed in the matrix before aging (Fig. 7a). A large number of $M_{23}C_6$ phases precipitate in the PAGB and lath boundary. After aging 100 h, TMLS changes into polygonal ferrite, and the size of the precipitate at the subgrain boundary is about 100 nm (point A). While after 300 h of high-temperature aging, a large precipitate appears with a size of 400 nm in the matrix (point B). Points A and B were calibrated by electron diffraction, and both the points were $M_{23}C_6$ carbide. During growth, because of the different lattice types, the parallel relationship disappears, the distortion energy increases, and the phase boundary grows with the lowest energy. The sticky precipitate is formed at last following Wulff's rule (Ref 39).

The restraining effect of the size of the precipitates on the migration of lath boundaries has been mentioned above. The fundamental reason is that the weakening of the pinning effect results in the significant migration of lath boundaries. The migration of lath boundaries leads to the transformation of martensite lath blocks into polygonal ferrite, and a large amount of precipitate are released. The growth of precipitates is also the key reason for transforming lath martensite into polygonal ferrite during high-temperature aging. Due to the transformation from lath martensite to fine polygonal ferrite, the number of small-angle grain boundaries after high-temperature aging for 300 h is similar to that before aging (Fig. 3e). The difference in the number of polygonal ferrites is due to the number of small-angle grain boundaries after aging at 650 °C for 300 h is lower than at 700 °C. The rate of this evolution is lower than 700 °C during the aging process at 650 °C. The increase in aging temperature could significantly accelerate the evolution of the microstructure.

3.3 Effect of Aging Condition on the Mechanical Properties

The results of mechanical properties at room temperature are shown in Fig. 8. It can be seen that before aging treatment, the yield strength of the sample is 633 MPa, and the elongation is 20.96%. After the first 100 h, the yield strength decreased, and the elongation, as well as the section shrinkage, increased. Then, the change in each index slowed down, and the whole trend was fast at first and then slowed down. After the same aging time, the sample's strength at 700 °C decreased, indicating that the microstructure's evolution speed is faster. Thus, the growth in the size of the precipitate is faster, and the dislocation movement is faster. The tensile strength of 9CrMoCoB steel after aging at 650 °C for 300 h reached 646 MPa, the yield strength reached 454 MPa, and the elongation reached 26.77%. Due to excellent comprehensive performance, 9CrMoCoB steel is recognized as heat-resistant steel for thermal power generation. Martensitic lath strengthening can provide higher

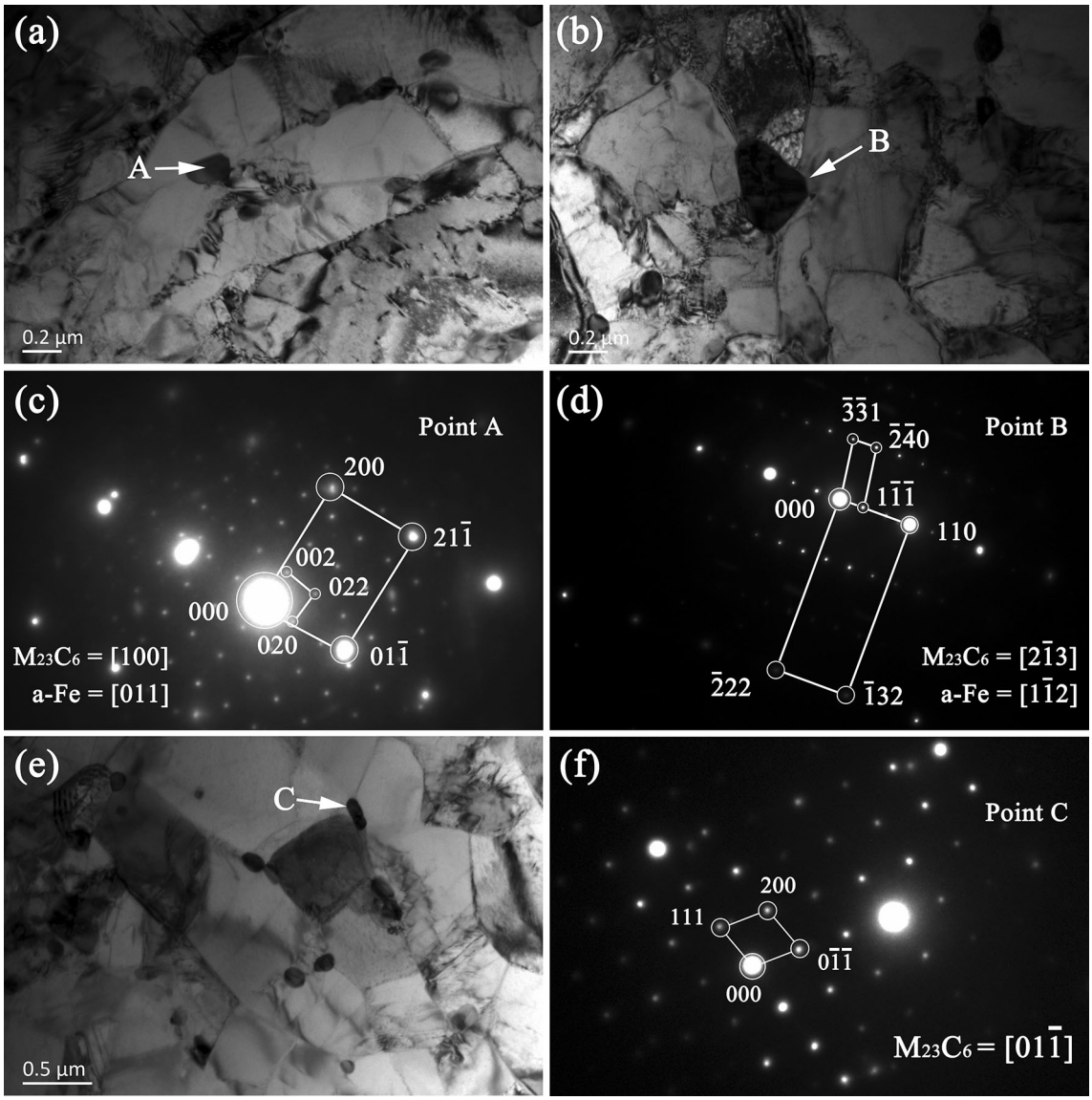

Fig. 7 TEM images of 9CrMoCoB steel after aging (a) 650 °C after 100 h (b) 650 °C after 300 h (c) diffraction pattern of (a); (b) diffraction pattern of (b); (e) 700 °C after 300 h (f) diffraction pattern of (e)

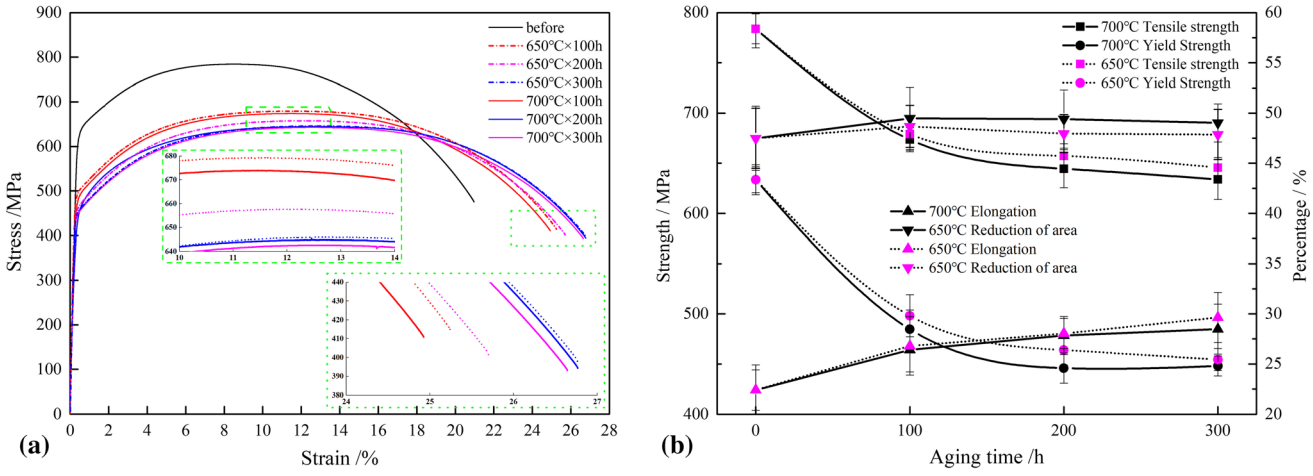

Fig. 8 The experimental results of the mechanical properties at room temperature (a) the tensile curves obtained under different conditions (b) mechanical data

strength and hardness, while precipitation strengthening can yield strength while also obtaining better plasticity. The above study identified that the growth of precipitates during high-temperature aging severely weakens the effects of grain boundary strengthening and lath martensite strengthening (Fig. 7). The experimental results from Fig. 8 well prove this effect.

The fracture surface of the tensile specimen is shown in Fig. 9. A large number of dimples are observed in the fracture, which is typical of the ductile fracture. The distribution of the dimple size is uniform. The small dimple is about 1 μm, and the large dimple is about 6 μm. The inclusions are not observed in the dimple. With an increase in the aging time, the fracture morphology did not change significantly. Precipitation was not observed in the dimple after aging for 300 h, although growth in the precipitate size was much larger than before aging. The precipitates did not support the breaking of the material after 300 h of high-temperature aging.

The high-temperature tensile strength and yield strength at 650 °C decreased with an increase in aging time (Fig. 10). But the strength of the steel sample after aging at 650 °C is higher than after 700 °C. The high-temperature tensile strength decreased from 326 to 252 MPa at 650 °C after 300 h. The high-temperature tensile strength decreased from 326 to 245 MPa at 700 °C after 300 h. The precipitate size has a significant effect on the tensile strength at high-temperature.

9CrMoCoB steel shows high tensile strength and yield strength before high-temperature aging. TMLS transforms into a polygonal ferrite after aging at 650 and 700 °C, as observed through TEM. The size of the precipitate significantly increased, and precipitate coarsening was found after aging for 200 h, which reduces the activation energy of the dislocation motion. It also facilitates the disappearance of TMLS and the generation of polygonal ferrite. The room

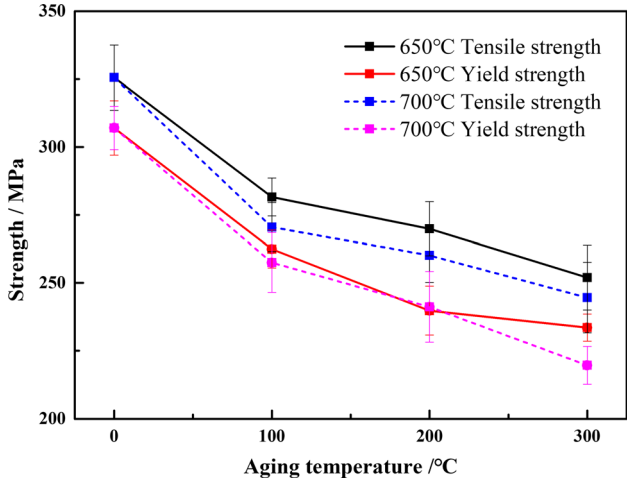

Fig. 10 Mechanical properties at high temperature under different aging conditions

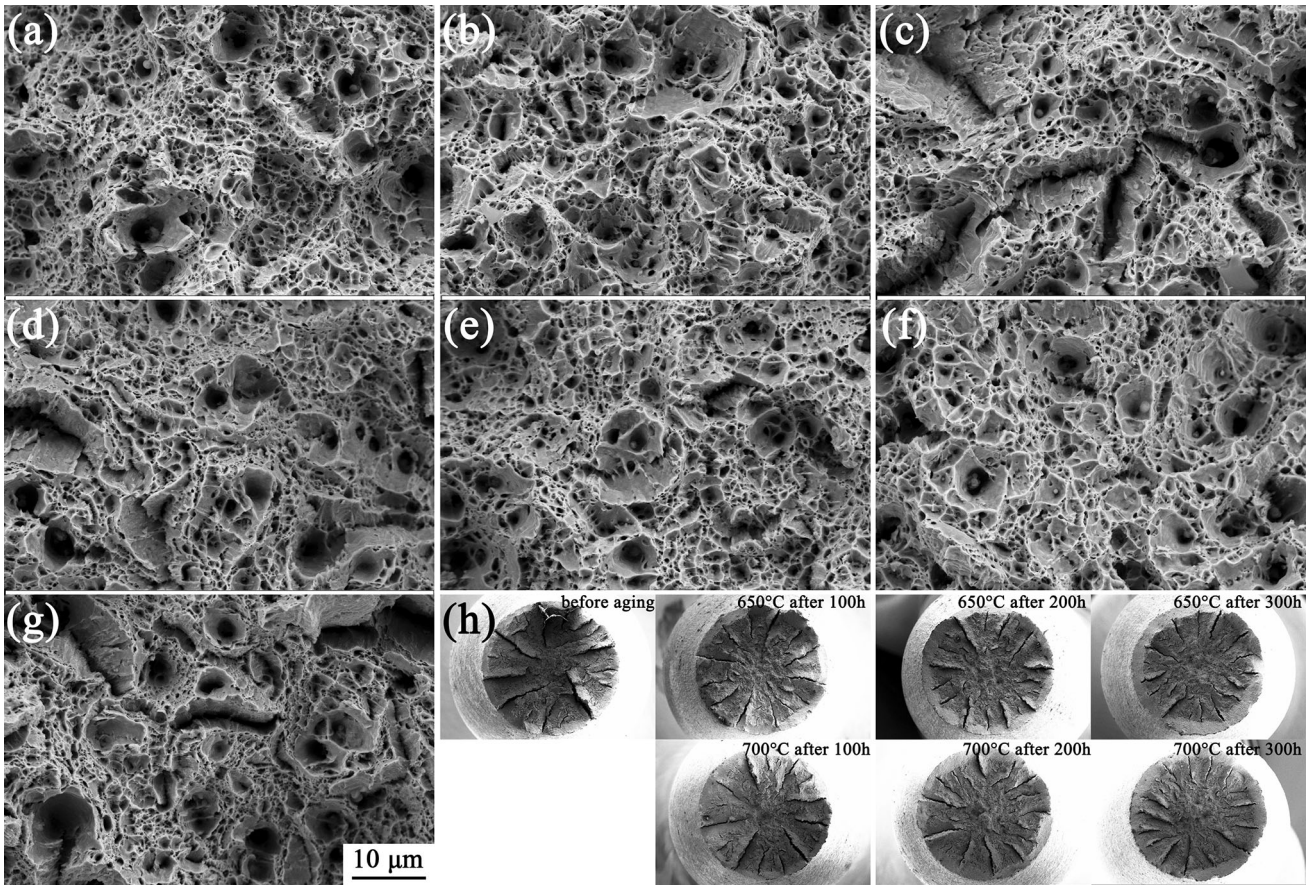

Fig. 9 Fracture surface morphology under different aging conditions (a) 650 °C after 100 h (b) 650 °C after 200 h (c) 650 °C after 300 h (d) 700 °C after 100 h (e) 700 °C after 200 h (f) 700 °C after 300 h (g) before aging (h) low magnification fracture morphology of each samples

temperature strength and high-temperature strength of 9CrMoCoB steel decreased in the static evolution in high-temperature aging. The coarsening of carbide precipitation is the main reason for reducing the strength of 9CrMoCoB steel during high-temperature aging.

4. Conclusions

In this study, the evolution in carbide precipitation and mechanical properties of 9CrMoCoB steel under different temperatures and holding times were studied. The main conclusions from this investigation are as follows:

1. After aging 300 h, TMLS in the matrix transformed to the polygonal ferrite, and the mean diameter of the precipitate increased from 183 to 267 nm at 650 °C, and increased from 183 to 302 nm at 700 °C.
2. In the aging process, the tensile strength decreased by 13.38 and 14.07% at 650 and 700 °C, respectively. During the first 100 h, they decreased by 1.77% and 1.66% in the final 100 h. The tensile strengths were 646 MPa and 634 MPa, respectively, after aging at 650 and 700 °C for 300 h. The yield strength was 633 MPa under the as-received condition, and after aging at 650 and 700 °C for 300 h, it was 454 and 448 MPa, respectively.
3. The growth of precipitates on the lath boundaries during high-temperature aging was the main reason for transforming lath martensite blocks to polygonal ferrite. The effect of this type of influence becomes significant after aging 200 h.

Acknowledgment

This investigation is supported by the following funds: the Liaoning Province Doctoral Research Startup Fund Project (2019-BS-168), the China Post-doctoral Science Foundation (grant no. 2019M661122), the Key Research and Development Program of Shaanxi (Program No.2019GY-151, 2019GY-178, 2020GY-251), the National Natural Science Foundation of China (51901193), Science and Technology Plan Project of Weiyang District in Xi'an City (201905), and the Science and Technology Project of Xi 'an (2020KJRC0141). The authors would like to express their gratitude to EditSprings (https://www.editsprings.com/) for the expert linguistic services.

References

1. Y. Liu, Y. Ma, H. Guo and C. Liu, Effects of Co and B on Microstructure and Properties of Modified Ferritic Heat-resistant Steels, *Materials Review*, 2015, **13**, p 003
2. R. Viswanathan, J.F. Henry, J. Tanzosh, G. Stanko, J. Shingledecker, B. Vitalis and R. Purgert, U.S. Program on Materials Technology for Ultra-Supercritical Coal Power Plants, *J. Mater. Eng. Perform.*, 2005, **14**(3), p 281–292
3. T.U. Kern, M. Staubli and B. Scarlin, The European Efforts in Material Development for 650 Degrees C USC Power Plants - COST522, *ISIJ Int.*, 2002, **42**(12), p 1515–1519. (**in English**)
4. C.H. Jia, C.X. Liu, Y.C. Liu, C. Li and H.J. Li, Microstructural Evolution and Constitutive Models of 9CrMoCoB Heat-Resistant Steel During High-Temperature Deformation, *J. Iron Steel Res. Int.*, 2019, **26**(11), p 1228
5. S.T. Mandziej and A. Vyrostkova, Creep and Fracture Behavior of Long-Annealed Weld HAZ in CB2 Steel, *Weld World*, 2020, **64**(3), p 573–590
6. Y. Chen, X. Lou, L. Yang, C. Wang, K. Zhou, M. Chen, Q. Wang, S. Zhu and F. Wang, Oxidation and Corrosion Protection of ZG12Cr9Mo1Co1NiVNbNB (CB2) Ferritic Stainless Steel by Inorganic Composite Coatings at 650° C, *Corros. Sci.*, 2020, **177**, p 109000
7. C. Jia, Y. Liu, C. Liu, C. Li and H. Li, Precipitates Evolution during Tempering of 9CrMoCoB (CB2) Ferritic Heat-Resistant Steel, *Mater. Charact.*, 2019, **152**, p 12–20
8. A. Vyrostkova, L. Falat, J. Kepic, P. Brziak, J. Pecha, Microstructure and Fracture of 9%Cr-Mo-Co-B Steel (Cb2) Weldment after Isothermal Ageing, *Metal 2010: 19th International Metallurgical and Materials Conference*, 409-414 (2010) (in English)
9. S. Baumgartner, M. Schuler, A. Holy, R. Schnitzer and N. Enzinger, Dissimilar Welding of the Creep Resistant steels CB2 and P92 with Flux Cored Wires, *Weld World*, 2015, **59**(5), p 655–665. (**in English**)
10. T.H. Hsiao, T.C. Chen, S.L. Jeng, T.J. Chung and L.W. Tsay, Effects of Simulated Microstructure on the Creep Rupture of the Modified 9Cr-1Mo Steel, *J. Mater. Eng. Perform.*, 2016, **25**(10), p 4317–4325. (**in English**)
11. X. Wang and X. He, Effect of Boron Addition on Structure and Properties of Low Carbon Bainitic Steels, *ISIJ Int.*, 2002, **42**(Suppl), p S38–S46
12. K.S. Chandravathi, K. Laha, N. Shinya, M.D. Mathew, Effects of Boron and Cerium on Creep Rupture Properties of Modified 9Cr-1Mo Steel and its Weld Joint, *6th International Conference on Creep, Fatigue and Creep-Fatigue Interaction*, **55**, 433-437 (2013) (in English)
13. X. Wang, L.F. Zhan, Q.G. Pan, Z.J. Liu, H. Liu and Y.S. Tao, Microstructure and Creep Properties of High Cr Resisting Weld Metal Alloyed with Co, *J Zhejiang Univ-Sc A*, 2010, **11**(10), p 756–760
14. H.R. Cui, F. Sun, K. Chen and J.S. Wu, Combined Effect of Co and W on Deformation Resistance of 12Cr Heat-Resistant Steel for USC Steam Turbines, *J. Mater. Eng. Perform.*, 2011, **20**(9), p 1613–1619. (**in English**)
15. K. Yamada, M. Igarashi, S. Muneki and F. Abe, Effect of Co Addition on Microstructure in High Cr Ferritic Steels, *ISIJ Int.*, 2003, **43**(9), p 1438–1443. (**in English**)
16. P. Yan, Z.D. Liu, H.S. Bao, Y.Q. Weng and W. Liu, Effect of Microstructural Evolution on High-Temperature Strength of 9Cr-3W-3Co Martensitic Heat Resistant Steel under Different Aging Conditions, *Mater. Sci. Eng. A*, 2013, **588**, p 22–28. (**in English**)
17. Z. Liu, Z. Liu, X. Wang and Z. Chen, Investigation of the Microstructure and Strength in G115 Steel with the Different Concentration of Tungsten During Creep Test, *Mater. Charact.*, 2019, **149**, p 95–104
18. A. Baltusnikas, I. Lukosiute, V. Makarevicius, R. Kriukiene and A. Grybenas, Influence of Thermal Exposure on Structural Changes of M23C6 Carbide in P91 Steel, *J. Mater. Eng. Perform.*, 2016, **25**(5), p 1945–1951. (**in English**)
19. G. Golanski, A. Zielinska-Lipiec, A. Zielinski and M. Sroka, Effect of Long-Term Service on Microstructure and Mechanical Properties of

Martensitic 9% Cr Steel, *J. Mater. Eng. Perform.*, 2017, **26**(3), p 1101–1107. (**in English**)
20. M. Okayasu and T. Shigeoka, Effect of Microstructural Characteristics on Mechanical Properties of Ferritic Stainless Steel, *J. Mater. Eng. Perform.*, 2019, **28**(11), p 6771
21. N. Saini, C. Pandey and M.M. Mahapatra, Effect of Normalizing Temperature on Fracture Characteristic of Tensile and Impact Tested Creep Strength-Enhanced Ferritic P92 Steel, *J. Mater. Eng. Perform.*, 2017, **26**(11), p 5414
22. J. Kasl and D. Jandova, Metallography of CB2 Steel Used for Cast Turbine Components, *Metallography Xv*, 2014, **782**, p 179–185. (**in English**)
23. L. Falat, V. Homolova, L. Ciripova, P. Sevc, A. Svoboda, Ageing Effects on Microstructure, Mechanical Properties, and Fracture Behaviour of 9Cr-1.5Mo-1Co-VNbBN Martensitic Steel Welded Joint for High Temperature Application, *Adv Mater Sci Eng*, (2017) (in English)
24. J. Kasl, S. Mikmekova and D. Jandova, SEM, TEM and SLEEM (Scanning Low Energy Electron Microscopy) of CB2 Steel After Creep Testing, *Iop Conf. Ser.-Mat. Sci.*, 2014, **55**, p 012008
25. D. Jandova, J. Kasl and E. Chvostova, Microstructure of CB2 Steel Before and After Long-term Creep Tests, *Metallography Xv*, 2014, **782**, p 311–318. (**in English**)
26. X.C. Hao, L. Zhang, C. Xiong, Y.C. Ma and K. Liu, Effect of Long-Term Aging at 760 Degrees C on Microstructure and Mechanical Properties of a Ni-Cr-W-Fe Alloy, *Acta Metall. Sin.*, 2015, **51**(7), p 807–814
27. X.F.F. Guo, J.M. Gong, Y. Jiang, X.W. Wang and Y.P. Zhao, Microstructures and High-temperature Mechanical Properties in 9Cr-0.5Mo-1.8WVNb Steel after Aging at 650 Degrees C, *Mater. High Temp.*, 2015, **32**(6), p 566–574
28. B. Wang, Z.D. Liu, S.C. Cheng, C.M. Liu and J.Z. Wang, Microstructure Evolution and Mechanical Properties of HR3C Steel during Long-term Aging at High Temperature, *J. Iron Steel Res. Int.*, 2014, **21**(8), p 765–773. (**in English**)
29. P. Duan, Z. Liu, S. Gu and S. Wang, Evolution in Microstructure and Mechanical Properties of Inconel 783 Alloy Bolts after Long Term High-Temperature Aging at 700° C, *Metals-Basel*, 2020, **10**(11), p 1440
30. M.-H. Ku, F.-Y. Hung, T.-S. Lui and J.-J. Lai, Enhanced Formability and Accelerated Precipitation Behavior of 7075 Al Alloy Extruded Rod by High Temperature Aging, *Metals-Basel*, 2018, **8**(8), p 648
31. A. Zielinski, G. Golanski and M. Sroka, Assessment of Microstructure Stability and Mechanical Properties of X10CrWMoVNb9-2 (P92) Steel After Long-Term Thermal Ageing for High-Temperature Applications, *Kovove Mater.*, 2016, **54**(1), p 61–70. (**in English**)
32. A. Aghajani, C. Somsen and G. Eggeler, On the Effect of Long-term Creep on the Microstructure of a 12% Chromium Tempered Martensite Ferritic Steel, *Acta Mater.*, 2009, **57**(17), p 5093–5106. (**in English**)
33. S. Li, Z. Eliniyaz, L. Zhang, F. Sun, Y. Shen and A. Shan, Microstructural evolution of delta ferrite in SAVE12 steel under heat treatment and short-term creep, *Mater. Charact.*, 2012, **73**, p 144–152
34. P. Yan, Z.D. Liu, H.S. Bao, Y.Q. Weng and W. Liu, Effect of Normalizing Temperature on the Strength of 9Cr-3W-3Co Martensitic Heat Resistant Steel, *Mater. Sci. Eng. A*, 2014, **597**, p 148–156. (**in English**)
35. F. Barcelo, J.L. Bechade and B. Fournier, Orientation Relationship in Various 9%Cr Ferritic/Martensitic Steels-EBSD Comparison between Nishiyama-Wassermann Kurdjumov-Sachs and Greninger-Troiano, *Phase Transit.*, 2010, **83**(8), p 601–614. (**in English**)
36. Y.T. Xu, X.Y. Zhang, Y.B. Tian, C. Chen, Y.J. Nan, H. He and M.J. Wang, Study on the Nucleation and Growth of M23C6 Carbides in a 10% Cr Martensite Ferritic Steel after Long-term Aging, *Mater. Charact.*, 2016, **111**, p 122–127. (**in English**)
37. L. Cipolla, H.K. Danielsen, D. Venditti, P.E. Di Nunzio, J. Hald and M.A.J. Somers, Conversion of MX Nitrides to Z-Phase in a Martensitic 12% Cr steel, *Acta Mater.*, 2010, **58**(2), p 669–679. (**in English**)
38. D.S. Bae, W.S. Jung, K.T. Hong and K.S. Lee, Precipitation Behavior of MX Phase in Cr-Mo-N-X(X=VNbTi) Ferritic Steels, *Mech. Beh. Mater. X Pts 1 and 2*, 2007, **345–346**, p 1553
39. D.A. Porter, K.E. Easterling, M. Sherif, Phase Transformations in Metals and Alloys, (Revised Reprint), CRC Press, 2009